FINITE ELEMENT MODELLING OF THE THERMO-MECHANICAL BEHAVIOUR OF A 9Cr MARTENSITIC STEEL

R. A. Barrett[1,3], P. E. O'Donoghue[2,3], S. B. Leen[1,3]

Abstract A multi-axial, unified sinh viscoplastic material model has been developed to model the behaviour of advanced materials subjected to high temperature cyclic loading. The material model accounts for rate-dependent effects related to high temperature creep and cyclic plasticity effects such as isotropic and kinematic hardening. The material model, which is capable of simulating both isothermal and anisothermal loading conditions, is implemented in a material user subroutine and validated against uniaxial test data. The results indicate that the multi-axial implementation performs well for both isothermal and anisothermal uniaxial loading conditions for as-new P91 steel.

1 Introduction

Next generation power plants are faced with the need to facilitate an ever increasing growth in renewable energy technologies. The unpredictable nature of renewable sources of energy, attempts to minimise CO_2 emissions and more widespread use of flexible combined cycle gas power plant, results in the need for fossil-fuel based power plant to operate with increased flexibility. Such a load-following mode of operation results in potentially large cyclic thermal gradients, which in turn, lead to increased thermo-mechanical fatigue (TMF) of plant components and a reduction in component life. Coupled with this increased TMF is the requirement to improve overall plant efficiency and hence reduce the level of CO_2 emissions. This may be

[1] Mechanical and Biomedical Engineering, College of Engineering and Informatics, NUI Galway, Ireland
Email: r.barrett2@nuigalway.ie, sean.leen@nuigalway.ie
[2] Civil Engineering, College of Engineering and Informatics, NUI Galway, Ireland
Email: padraic.odonoghue@nuigalway.ie
[3] Ryan Institute for Environmental, Marine and Energy Research, NUI Galway, Ireland

achieved through the use of an ultra-supercritical (USC) cycle, with plant components subjected to increased steam pressure and temperature. With Type IV cracking already observed in plant components operating under a subcritical cycle [17], there is a need for the development of accurate life prediction methods for power plant components. To achieve this, effective and efficient computational methods are required to predict the life of plant components. This, in turn, requires material models which can accurately describe the constitutive behaviour of candidate materials, such as 9Cr steels, under high temperature loading.

The material model must have the capability to simulate, on the one hand, the rate-dependent effects associated with high temperature creep, while also maintaining the ability to model phenomena related to cyclic loading conditions, such as the Bauschinger effect and isotropic hardening. Thus, a unified viscoplasticity approach is required to model the creep-fatigue interaction observed in 9Cr steels. A number of models capable of dealing with the high temperature creep-fatigue interaction have been proposed, such as uniaxial implementations of the Chaboche power law model [3, 9, 10, 15, 20, 21], the two layer viscoplasticity model [6] and the MATMOD model [13]. The model proposed in the current study is a multi-axial sinh formulation. The sinh formulation is beneficial for a number of reasons. Firstly, as 9Cr steels display a linear stress-strain rate relationship at low stresses and strain rates and an exponential relationship at higher values, the sinh formulation allows for reliable interpolation and extrapolation beyond the limited experimental data available. Secondly, the mechanisms which dominate deformation vary from diffusion based creep at low stresses and high temperature to dislocation based creep at higher stresses [8]. As the low stress regime corresponds to Nabarro-Herring creep with an exponent of unity and the higher stress regimes are represented by power law creep with an exponent of up to 11 [18], the use of a sinh formulation allows for smooth transition from one phenomena to another.

The sinh material model is implemented both uniaxially and multi-axially. The multi-axial implementation is developed in a user material subroutine, for use with the commercial finite element (FE) code Abaqus. This study presents the first step in assessing the performance of the multi-axial material model by validating against uniaxial isothermal fatigue data [10] and uniaxial TMF test data [15] available in the literature.

2 Material Model

The sinh unified viscoplastic material model described in this study allows for accurate modelling of the isotropic and kinematic hardening phenomena associated with cyclic loading and the creep effects related to high temperature loading. This is achieved through the use of the following constitutive equation for the effective accumulated plastic strain rate [4]:

$$\dot{p} = \alpha \sinh \beta \left(J(\boldsymbol{\sigma} - \boldsymbol{\chi}) - R - k \right) \tag{2.1}$$

where $J(\boldsymbol{\sigma}\text{-}\boldsymbol{\chi})$ is the von Mises effective stress function, R is the isotropic hardening parameter, k is the initial yield stress, $\boldsymbol{\chi}$ is the back-stress tensor and α and β are temperature-dependent, viscoplastic material parameters. The material model uses an implicit integration scheme to evaluate the increment of effective plastic strain. The nature of the implicit scheme used in this model dictates that a trial stress is used to check for viscoplastic behaviour. This allows for the potential to be evaluated at the current timestep and the use of a radial return method [4] applies plastic correction to the value of trial stress obtained.

2.1 Material Model Development

Assuming only small strains apply, classical additive decomposition of strain gives the following equation for the total strain, $\boldsymbol{\varepsilon}$:

$$\boldsymbol{\varepsilon} = \boldsymbol{\varepsilon}^{\mathrm{el}} + \boldsymbol{\varepsilon}^{\mathrm{pl}} + \boldsymbol{\varepsilon}^{\mathrm{th}} \tag{2.2}$$

where $\boldsymbol{\varepsilon}^{\mathrm{el}}$ corresponds to the elastic strain, $\boldsymbol{\varepsilon}^{\mathrm{pl}}$ is the plastic strain and $\boldsymbol{\varepsilon}^{\mathrm{th}}$ is the thermal strain. The increment in stress, $\Delta\boldsymbol{\sigma}$, is calculated using the multi-axial form of Hooke's law, coupled with equation (2.2) written in terms of the elastic strain:

$$\Delta\boldsymbol{\sigma} = 2\mu\left(\Delta\boldsymbol{\varepsilon} - \Delta\boldsymbol{\varepsilon}^{\mathrm{th}}\right) + \lambda \mathrm{Tr}\left(\Delta\boldsymbol{\varepsilon} - \Delta\boldsymbol{\varepsilon}^{\mathrm{th}}\right)\mathbf{I} - 2\mu\Delta\boldsymbol{\varepsilon}^{\mathrm{pl}} \tag{2.3}$$

where λ and μ are Lamé's constants. In equation (2.3), the first two terms on the right hand side give the trial stress and the final term corresponds to the applied plastic correction. The increment of plastic strain, $\Delta\boldsymbol{\varepsilon}^{\mathrm{pl}}$, is determined by the flow rule:

$$\Delta\boldsymbol{\varepsilon}^{\mathrm{pl}} = \Delta p \mathbf{n} \tag{2.4}$$

where $\mathbf{n}$ represents the tensor normal and Δp corresponds to the increment in effective plastic strain. For a von Mises material, the tensor normal is defined by the following equation:

$$\mathbf{n} = \frac{\partial \sigma_{\mathrm{v}}}{\partial \boldsymbol{\sigma}} = \frac{3}{2}\frac{\mathbf{S} - \boldsymbol{\chi}}{\mathrm{J}(\boldsymbol{\sigma} - \boldsymbol{\chi})} \tag{2.5}$$

In equation (2.5), σ_v is the viscous stress and $\mathbf{S}$ is deviatoric stress. The viscous stress is defined as:

$$\sigma_{\mathrm{v}} = J(\boldsymbol{\sigma} - \boldsymbol{\chi}) - R - k \tag{2.6}$$

Nonlinear kinematic hardening, which accounts for translation of the centre of the elastic domain in 3D stress space, is described by a summation of Armstrong-Frederick type back-stress tensors [2, 11]:

$$\boldsymbol{\chi} = \boldsymbol{\chi}_1 + \boldsymbol{\chi}_2 \tag{2.7}$$

$$\dot{\boldsymbol{\chi}}_{\mathrm{i}} = \frac{2}{3} c_{\mathrm{i}} \dot{\boldsymbol{\varepsilon}}^{\mathrm{pl}} - \gamma_{\mathrm{i}} \boldsymbol{\chi}_{\mathrm{i}} \dot{p} + \frac{1}{c_{\mathrm{i}}} \frac{\partial c_{\mathrm{i}}}{\partial T} \boldsymbol{\chi}_{\mathrm{i}} \dot{T} \tag{2.8}$$

where T is temperature and c_i and γ_i are temperature-dependent material parameters. The three terms in equation (2.8) correspond to (i) a linear kinematic hardening term, (ii) a recall term and (iii) a temperature rate term, respectively. $\boldsymbol{\chi}_1$ accounts for the kinematic behaviour at lower strain hardening levels and $\boldsymbol{\chi}_2$ for higher levels of strain hardening. The variable R takes into account the expansion/contraction of the elastic domain and is given by the following relationship [11, 22]:

$$\dot{R} = b\left(Q - R\right)\dot{p} + \left(\frac{1}{b}\frac{\partial b}{\partial T} + \frac{1}{Q}\frac{\partial Q}{\partial T}\right)R\dot{T} \tag{2.9}$$

where b and Q are temperature-dependent material parameters representing the decay rate and the saturation value of R respectively. In equations (2.8) and (2.9), the temperature-rate terms account for the effects of anisothermal loading conditions and the variations of the material parameters b, Q and c_i as functions of temperature.

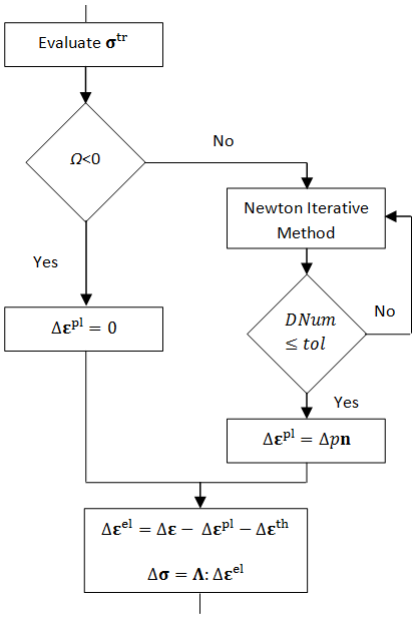

Figure 1: Flowchart of the material user subroutine process.

The sinh formulation defined above has been implemented in uniaxial form in a stand-alone computer program and also multi-axially within a user material (UMAT) subroutine in the general-purpose, non-linear FE code Abaqus. Figure 1 depicts a flowchart of the main processes involved in the subroutine. Once the equivalent trial stress has been obtained, a check for viscoplastic behaviour on the current timestep is conducted. Viscoplastic behaviour is implemented ($\dot{\boldsymbol{\varepsilon}}^{\mathbf{pl}} \neq 0$) if the following criterion is met:

$$\Omega \geq 0 \quad \text{and} \quad \frac{\partial \sigma_v}{\partial \boldsymbol{\sigma}} : \dot{\boldsymbol{\sigma}} \geq 0 \tag{2.10}$$

where Ω is the dissipation potential, defined for the hyperbolic sine model as:

$$\Omega = \frac{\alpha}{\beta}\cosh(\beta\sigma_v)\mathrm{sgn}(\beta\sigma_v) \tag{2.11}$$

If viscoplastic behaviour is observed, a Newton iterative method is employed to obtain a converged increment in effective plastic strain and the increments of the plastic strain tensor are evaluated using the flow rule, described by equation (2.4). The increment of stress is then calculated using the simple constitutive equation:

$$\Delta\boldsymbol{\sigma} = \boldsymbol{\Lambda} : \left(\Delta\boldsymbol{\varepsilon} - \Delta\boldsymbol{\varepsilon}^{pl} - \Delta\boldsymbol{\varepsilon}^{th}\right) \tag{2.12}$$

where $\boldsymbol{\Lambda}$ is the standard elasticity matrix.

2.2 Material Model Parameters

This paper is primarily concerned with the multi-axial implementation of a hyperbolic sine unified viscoplasticity model for cyclic stress-strain rate dependence and with preliminary identification of the salient hyperbolic material parameters, α and β, for the TMF behaviour of as-new P91. To this end, the published stress relaxation data of Koo et al. [10] for temperatures of 500 °C and 600 °C and the isothermal cyclic data of Saad et al. [15] for P91 steel, between 400 °C and 600 °C are employed. The experimental cyclic data of Saad et al. [15] is obtained at a strain rate of 0.1 %/*s* and a strain range of ±0.5 %. The first step is calibration of the material parameters. This is achieved using the stand-alone uniaxial code. Three sets of constants are identified, namely (i) elastic constants, Young's modulus (E), Poisson's ratio (v, taken as 0.3 throughout), initial yield stress (k) and the coefficient of thermal expansion (α_{COE}), (ii) kinematic and isotropic hardening parameters and (iii) the viscoplastic hyperbolic parameters. For P91 steel, the temperature-dependent parameters for (i) are published by ASME [1] and are given in Table 1. The present model is essentially a variation of the unified Chaboche model, with (i) a hyperbolic viscoplasticity function replacing the power-law function and (ii) inclusion of additional temperature-rate terms for the isotropic and kinematic hardening functions, but otherwise with similar isotropic and kinematic hardening evolution functions. Hence, for the current study, the kinematic and isotropic hardening parameters of [15] are adopted in general. Note that the initial yield stress value, k, at 600 °C is however, lower than that of [15], as calibration of the relaxation data of Koo et al. [10] led to a modified value of 43 MPa for this. As it is well documented that P91 steel undergoes cyclic softening behaviour due to coarsening of the microstructure [7, 15, 16], the isotropic hardening parameter Q has a negative value.

From this initial material data, an iterative process is undertaken within the uniaxial code, whereby preliminary values of the hyperbolic parameters, α and β, are obtained by comparison with stress relaxation data [10] and isothermal cyclic data [15]. The resulting temperature-dependent values are listed in Table 3. Piece-wise linear interpolation is used to evaluate the material constants for the anisothermal cases.

Table 1: Published temperature-dependent values of Young's modulus and coefficient of thermal expansion for as-new P91 steel [1].

$\boldsymbol{Temperature}$ $(°\boldsymbol{C})$	$\boldsymbol{E}$ $(\boldsymbol{GPa})$	$\boldsymbol{\alpha_{COE}}(/℃)$
400	184	12.95×10^{-6}
500	163	13.31×10^{-6}
600	142	13.59×10^{-6}

Table 2: Isotropic and kinematic hardening parameters for as-new P91 steel [15].

$\boldsymbol{T}$ $(°\boldsymbol{C})$	$\boldsymbol{k}$ $(\boldsymbol{MPa})$	$\boldsymbol{Q}$ $(\boldsymbol{MPa})$	$\boldsymbol{b}$	$\boldsymbol{C_1}$ $(\boldsymbol{MPa})$	$\boldsymbol{\gamma_1}$	$\boldsymbol{C_2}$ $(\boldsymbol{MPa})$	$\boldsymbol{\gamma_2}$
400	96	−55.0	0.45	352500.0	2350.0	48600.00	405.0
500	90	−60.0	0.60	215872.6	2191.6	48235.29	460.7
600	43	−75.4	1.00	106860.0	2055.0	31159.90	463.0

Table 3: Temperature-dependent hyperbolic material parameters for as-new P91 steel.

Temperature (℃)	**α (s^{-1})**	**β (MPa^{-1})**
400	8×10^{-07}	0.07
500	4×10^{-07}	0.064
600	1×10^{-07}	0.055

3 Results

The uniaxial code has been successfully calibrated against the previously published experimental results of [10, 15] and the multi-axial UMAT hyperbolic implementation has, in turn, been successfully validated against (i.e. gave identical results to) the uniaxial stand-alone hyperbolic code. The details are not shown here for compactness. The results of the calibration process are illustrated in Figure 2a and Figures 3 and 4. Following calibration using the uniaxial code, the next steps are (i) validation of the multi-axial FE-implementation for isothermal (uniaxial) strain-controlled test conditions for P91 steel, and (ii) investigation of the validity of the isothermally-identified parameters for anisothermal (TMF) test conditions for P91 steel, including initial assessment of the effects of the additional temperature-rate terms over the range of test conditions from [10, 15].

Validation of the performance of the multi-axial material model for uniaxial isothermal cyclic loading conditions is conducted against data available in the literature [10, 15]. Figure 2b depicts the results obtained for a stress relaxation test at a temperature of 500 °C for the conditions tested in [15] and Figure 5 illustrates the isothermal cyclic results obtained at a temperature of 500 °C for a different strain rate of 0.01 %/s, where excellent agreement with the experimental data is obtained. A similar quality of correlation is achieved for isothermal modelling at

400 °C. As expected, P91 steel exhibits considerable cyclic softening, with a 22% reduction in the stress range for isothermal loading at 600 °C, for example.

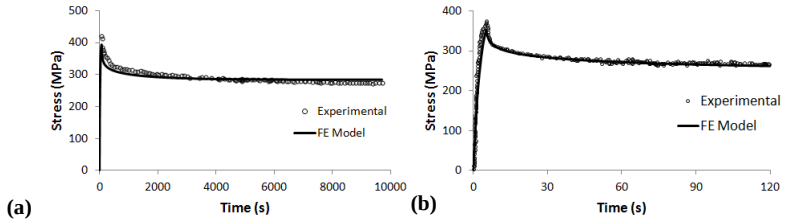

Figure 2: Stress relaxation tests at 500°C for (a) calibration of the hyperbolic viscoplastic parameters from the data of Koo et al.[10] and (b) validation against data of Saad et al. [15].

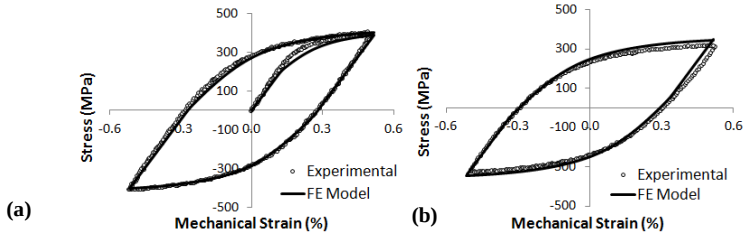

Figure 3: Calibration of the material parameters from the experimental data of Saad et al. [15] at 500 °C and a strain rate of 0.1 %/s for (a) the initial cycle and (b) after 600 cycles.

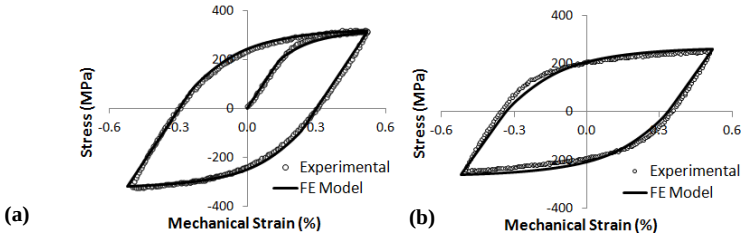

Figure 4: Calibration of the material parameters from the experimental of data Saad et al. [15] at 600 °C and a strain rate of 0.1 %/s for (a) the initial cycle and (b) after 300 cycles.

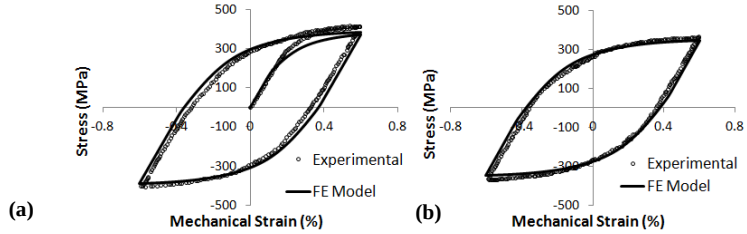

Figure 5: Validation comparison of FE-predicted and the experimental data of Koo et al. [10] at 500 °C and a strain rate of 0.01 %/s for (a) the initial cycle and (b) after 130 cycles.

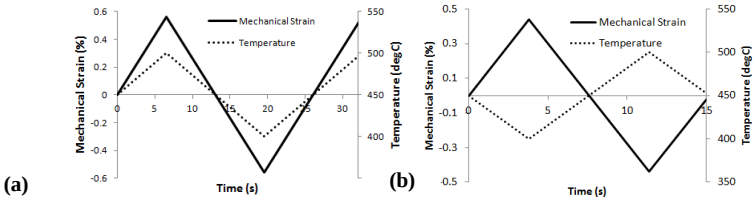

Figure 6: Loading conditions for (a) TMF-IP loading and (b) TMF-OP loading.

Figure 6 shows the in-phase (IP) and out-of-phase (OP) anisothermal loading conditions simulated within the present study. Figure 7 illustrates that good correlation is achieved between the FE and measured [15] stress-strain responses for IP loading in the 400 to 500 ℃ range. Similar results are obtained for the 400 to 600 ℃ IP case, as shown in Figure 8, although the model over-predicts stress range by about 5%, at the tensile side, for later cycles. Figure 9 shows that the model performs well for the early cycles for the 400 to 500 ℃ OP case; however, it slightly over-predicts stress range (~10%) for later cycles, but still captures the tensile peak accurately.

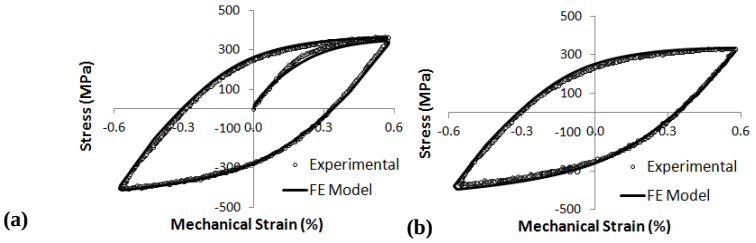

Figure 7: Comparison of FE-predicted and measured [15] hysteresis loops for 400 to 500 °C TMF-IP loading, for (a) the initial loop and (b) after 100 cycles.

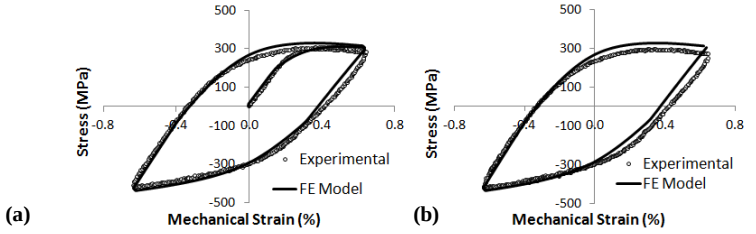

Figure 8: Comparison of FE-predicted and measured [15] hysteresis loops for 400 to 600 °C TMF-IP loading, for (a) the initial loop and (b) after 3 cycles.

4 Discussion and Conclusions

For the strain rates and strain ranges considered, the FE implementation of a multi-axial hyperbolic sine material model results in good correlation with both the experimental data and the unified Chaboche model implementations of [10, 15]. For the isothermal conditions simulated from 500 to 600 °C, the results show excellent

agreement with the experimental data; discrepancies within the results may be attributable to non-optimised material parameters.

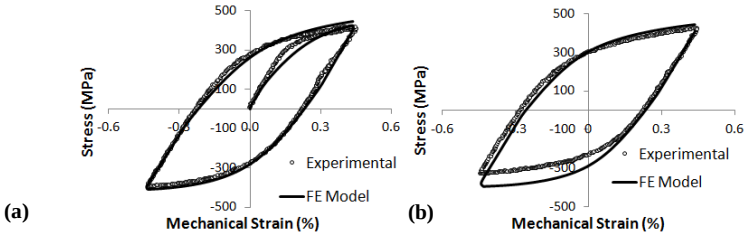

Figure 9: Comparison of FE-predicted and measured [15] hysteresis loops for 400 to 500 °C TMF-OP loading, for (a) the initial loop and (b) after 100 cycles.

It has been argued (e.g. [5, 14]) that the hyperbolic sine viscoplasticity function, as compared to the power-law function of the unified Chaboche model, is (i) more representative of the mechanisms of deformation for martensitic-ferritic steels at high temperature, spanning a range of loading levels, e.g. cyclic loading, and (ii) therefore, has potential benefits for interpolation and extrapolation from the limited test conditions, typically employed for constitutive parameter identification, to the broader range of stress, strain-rate and temperature conditions experienced by real-plant components, as particularly required for ever-more flexible plant operation. This benefit has been alluded to within the present study by the ability of the hyperbolic sine material model to simulate the behaviour of P91 steel at different strain rates (e.g. see Figures 3 and 5). Further validation of the multi-axial capability of the material model is required in future work, for example, by comparison with notched specimen data, e.g. see [19]. The ultimate aim is for application to realistic plant operating conditions for identification of representative TMF conditions for testing, e.g. see [5] and life prediction.

For the case of anisothermal loading conditions, the predicted results, which are also similar to those of the unified Chaboche model [15], suggest that the isothermal identification of material parameters is a reasonable basis for subsequent anisothermal behaviour prediction. The IP predictions are superior to the OP predictions, particularly for later OP cycles. The additional temperature-rate terms (i.e. the temperature derivative terms on the right hand side of equations 2.8 and 2.9) have been found, for the conditions studied here, to lead to a reasonably small effect on stress range, typically about 6%. It is proposed that the use of a global optimisation technique, such as [12], in future work will allow more detailed identification of the material parameters.

Acknowledgements

This publication has emanated from research conducted with the financial support of Science Foundation Ireland under Grant Number SFI/10/IN.1/I3015. SBL gratefully acknowledges receipt of a Millennium Travel Grant from NUI Galway. Helpful discussions with Prof. Noel O'Dowd of the Materials and Surface Science Institute (MSSI) of the University of Limerick are also acknowledged.

References

1. ASME Boiler and Pressure Vessel Code, 1998. Section II, Part D, ASME, New York (1998).
2. Chaboche, J.L. Int. J. Plasticity 24 (2008) 1642-1693.
3. Chaboche, J.L., Rousselier, G. Int. J. Pressure Vessel Tech. 105 (1983) 153-158.
4. Dunne, F., Petrinic, N., 2005. *Introduction to Computational Plasticity*. Oxford: Oxford University Press.
5. Dyson, B.F., Osgerby, S. NPL Report, DMM(A) 116, 1993.
6. Farragher, T.P., Scully, S., O'Dowd, N.P., Leen, S.B. Int. J. Pressure Vessel Tech. (2012) - Article in press.
7. Fournier, B., Sauzay, M., Barcelo, F., Rauch, E., Renault, A., Cozzika, T., Dupuy, L., Pineau, A. Metallurgical and Materials Transactions A, 40 (2009) 330-341.
8. Hertzberg, R. W., 1996. *Deformation and Fracture Mechanics of Engineering Materials*. New York: John Wiley & Sons, Inc.
9. Hyde, C.J., Sun, W., Leen, S.B. Int. J. Pressure Vessels and Piping 87 (2010) 29-33.
10. Koo, G.H., Kwon, J.H. Int. J. Pressure Vessels and Piping 88 (2011) 26-33.
11. Lemaitre, J., Chaboche, J. L, 1994. *Mechanics of Solid Materials*. Cambridge: Cambridge University Press.
12. Mahmoudi, A.H., Pezeshki-Najafabadi, S.M., Badnava, H. Computational Materials Science 50 (2011) 1114-1122.
13. Miller, A.K., 1987. *Unified Constitutive Equations for Creep and Plasticity*. New York: Elsevier Applied Science Publishers Ltd.
14. Perrin, I.J., Hayhurst, D.R. J. of Strain Analysis 31 (1996) 299-314.
15. Saad, A.A., Hyde, C.J., Sun, W., Hyde, T.H. Materials at High Temperature 28 (3) (2011) 212-218.
16. Saad, A.A., Sun, W., Hyde, T.H., Tanner, D.W.J. Procedia Engineering 10 (2011) 1103-1108.
17. Scully, S., ESB Energy International, personal communication, February (2012).
18. Shrestha, T., Basirat, M., Charit, I., Potirniche, G.P., Rink, K.K., Sahaym, U. Journal of Nuclear Materials 423 (2012) 110-119.
19. Tanner, D.W.J., Sun. W., Hyde, T.H. Procedia Engineering 10 (2011) 1081-1086.
20. Tong, J., Vermeulen, B. Int. J. Fatigue 25 (2003) 413-420.
21. Zhan, Z. A study of creep-fatigue interaction in a new nickel-based superalloy. PhD thesis, University of Portsmouth, 2004.
22. Zhang, Z., Delagnes, D., Bernhart, G. Int. J. Fatigue 24 (2002) 635-648.